Society for Mathematical Biology

ORIGINAL ARTICLE



Modeling the Mechanisms by Which Coexisting Biomolecular RNA–Protein Condensates Form

K. Gasior^{1,2} · M. G. Forest^{2,3,4} · A. S. Gladfelter⁵ · J. M. Newby⁶

Received: 25 January 2020 / Accepted: 21 October 2020 / Published online: 24 November 2020 © Society for Mathematical Biology 2020

Abstract

Liquid-liquid phase separation is an emerging mechanism for intracellular organization. This work presents a mathematical model to examine molecular mechanisms that yield phase-separated droplets composed of different RNA-protein complexes. Using a Cahn-Hilliard diffuse interface model with a Flory-Huggins free energy scheme, we explore how multiple (here two, for simplicity) protein-RNA complexes (species) can establish a heterogeneous droplet field where droplets with single or multiple species phase separate and evolve during coarsening. We show that the complex-complex de-mixing energy tunes whether the complexes co-exist or form distinct droplets, while the transient binding kinetics dictate both the timescale of droplet formation and whether distinct species phase separate into droplets simultaneously or sequentially. For specific energetics and kinetics, a field of droplets driven by the formation of only one protein-RNA complex will emerge. Slowly, the other droplet species will accumulate inside the preformed droplets of the other species, allowing them to occupy the same droplet space. Alternatively, unfavorable species mixing creates a parasitic relationship: the slow-to-form protein-RNA complex will accumulate at the surface of a competing droplet species, siphoning off the free protein as it is released. Once this competing protein–RNA complex has sufficiently accumulated on the droplet surface, it can form a new droplet that is capable of sharing an interface with the first complex droplet but is not capable of mixing. These results give insights into a wide range of phase-separation scenarios and heterogeneous droplets that coexist but do not mix within the nucleus and the cytoplasm of cells.

Keywords Liquid–liquid phase separation · Flory–Huggins · RNA–protein dynamics · Phase field model

Extended author information available on the last page of the article



[☑] J. M. Newby jnewby@ualberta.ca

153 Page 2 of 16 K. Gasior et al.

1 Introduction

Liquid-liquid phase separation (LLPS) has emerged as a common mechanism for intracellular organization in both the cytoplasm and the nucleus (Langdon and Gladfelter 2018). These membrane-less compartments exhibit properties similar to those of liquid-like droplets (Hyman et al. 2014, Elbaum-Garfinkle et al. 2015) and it is hypothesized that these droplets create localized environments to facilitate cellular processes, such as those performed by RNA-protein complexes (Langdon and Gladfelter 2018). Many proteins involved in LLPS are intrinsically disordered with polyglutamine (polyQ) tracts (Schaefer et al. 2012), prion-like domains (Tetz and Tetz 2017), or low-complexity sequences that promote phase separation (Lee et al. 2015; Molliex et al. 2015; Feric et al. 2016; Pak et al. 2016). Additionally, these intrinsically disordered domains are commonly adjacent to RNA-binding domains (Molliex et al. 2015, Chong et al. 2018). Due to the multivalent nature of these proteins and the RNA they bind with (Lin et al. 2015, Banani et al. 2017, Langdon et al. 2018), there may be highly complex combinations of protein-RNA complexes within the cell and the distributions of these different forms of complexes likely vary throughout the dynamics of the LLPS process.

Within the cellular environment, intrinsically disordered RNA-binding proteins can interact with many different species of RNA. Depending upon the RNA sequence involved, the droplets formed by the RNA-protein complexes can have different properties and functions in cells (Lee et al. 2013a, b, Lee et al. 2015, Langdon et al. 2018). One example arises in the multinucleated branching fungal cell, Ashbya gossypii (Gladfelter 2006). In Ashbya, the protein Whi3 can bind with several different RNA sequences, including but not limited to a cell cycle factor CLN3 that encodes a cyclin protein (Lee et al. 2013a), and a cell polarity factor BNII that encodes an F-actin nucleator (Lee et al. 2015). Droplets formed between the binding of *CLN3* to Whi3 are located around the different nuclei in the cell and are involved in maintaining asynchronous nuclear division (Lee et al. 2013a). Droplets formed due to the interactions between BNI1 and Whi3 are located at the tips and branching sites of the cell and are involved in cellular polarity (Lee et al. 2015). Through in vitro experiments, the Gladfelter Lab established that CLN3-Whi3 droplets have a higher viscosity than BNII-Whi3 droplets (Zhang, Elbaum-Garfinkle et al. 2015). Additionally, it was further shown that CLN3-Whi3 droplets exclude the BNII-Whi3 complex, forming two distinct droplet species. This lack of mixing is due to conformational changes in the RNA structure, partially induced by the RNA interactions with Whi3 (Langdon et al. 2018). This simple "two RNA, one protein" system is an excellent model system to build a mechanistic understanding of how the molecular identity of droplets is established—the focus of this paper.

Phase separations and the molecular interactions that promote them have been extensively explored through mathematical modeling. These models utilize both sharp and diffuse interface techniques to understand how transient protein–RNA interactions can create both microscopic and macroscopic changes within the cytoplasmic or nuclear environment (Glotzer et al. 1995; Lee et al. 2013a, b; Zwicker et al. 2017; Berry et al. 2018; Gasior et al. 2019). Analogous dynamic chromosomal architectures due to transient gene–gene crosslinks have been predicted and experimentally vali-



dated using stochastic molecular dynamics models of entropic polymers (Hult et al. 2017; Walker et al. 2019). Further, recent work by Gasior et al. (2019) established a modeling framework to understand how bivalent interactions between a protein and single RNA species can influence intra-droplet patterning. Using the Cahn–Hilliard diffuse interface model (Cahn and Hilliard 1958) paired with a modified double-well free energy, this phase-field model examined how competition for a shared resource and the bivalent nature of protein–RNA complexes can create a shell-core intra-droplet pattern both at the onset of phase separation and in the subsequent behavior of the system. The main conclusion of the study was that the molecular interaction rates, combined with phase-dependent diffusion, dictate spatial patterning and organization within the droplets.

While Gasior et al. focused on the competition between bivalent RNA-protein interactions that tunes intra-droplet patterning, here we examine a different molecular relationship known to occur in cells: the sharing of a common protein-binding partner by multiple RNA species. In this work, we seek to mechanistically understand how multiple RNA species can localize to distinct, individual droplets, creating a heterogeneous droplet field, despite the fact that they share a common binding partner. As in [19], we use the Cahn-Hilliard diffuse interface model (Cahn and Hilliard 1958; Qin and Bhadeshia 2010). However, instead of a modified double-well chemical potential, here we use the Flory-Huggins free energy scheme (Dudowicz et al. 2004; Brangwynne et al. 2015; Berry et al. 2018; Weber et al. 2019). In doing so, we are able to explore the diversity of scenarios that result from the mixing/de-mixing energy between distinct protein-RNA complexes, as well as the complex mixing propensity with the surrounding matrix. Additionally, this free energy scheme allows us to explore how these relationships, coupled with the transient binding kinetics of the complexes, regulate the membrane-less compartments whereby distinct complexes can individually phase separate into distinct droplets, co-exist within the same droplet, or evolve into droplet pairs with a shared interface where proteins are drawn from one complex to populate the other.

Ultimately, this work shows that multiple molecular mechanisms work together to establish a heterogeneous droplet field. In particular, we find that the de-mixing energy between the two complexes $(\chi_{K_1K_2})$ determines whether different species co-localize in a single droplet, while the binding kinetics dictate the timescale on which the droplet field develops. The two RNA-protein complexes must favor de-mixing from each other to observe the emergence of distinct droplet species. However, with certain binding dynamics, we still may observe only a single droplet species initially driving phase separation. The initial emergence of a single droplet species concentrates the shared protein resource and, in a system that favors the de-mixing of the two complexes, a parasitic relationship subsequently develops. The slow-to-form protein-RNA complex will accumulate at the surface of a competing droplet species, siphoning off the free protein as it is released. Once this competing protein–RNA complex has sufficiently accumulated it fails to mix with the RNA-protein species and, instead, forms its own droplets via budding or Ostwald ripening. Thus, while a single species initiates phase separation, there is a subsequent emergence of the second complex that can share an interface with the initial species; within that interface, the protein mixes between the droplets while the complexes remain separated.



153 Page 4 of 16 K. Gasior et al.

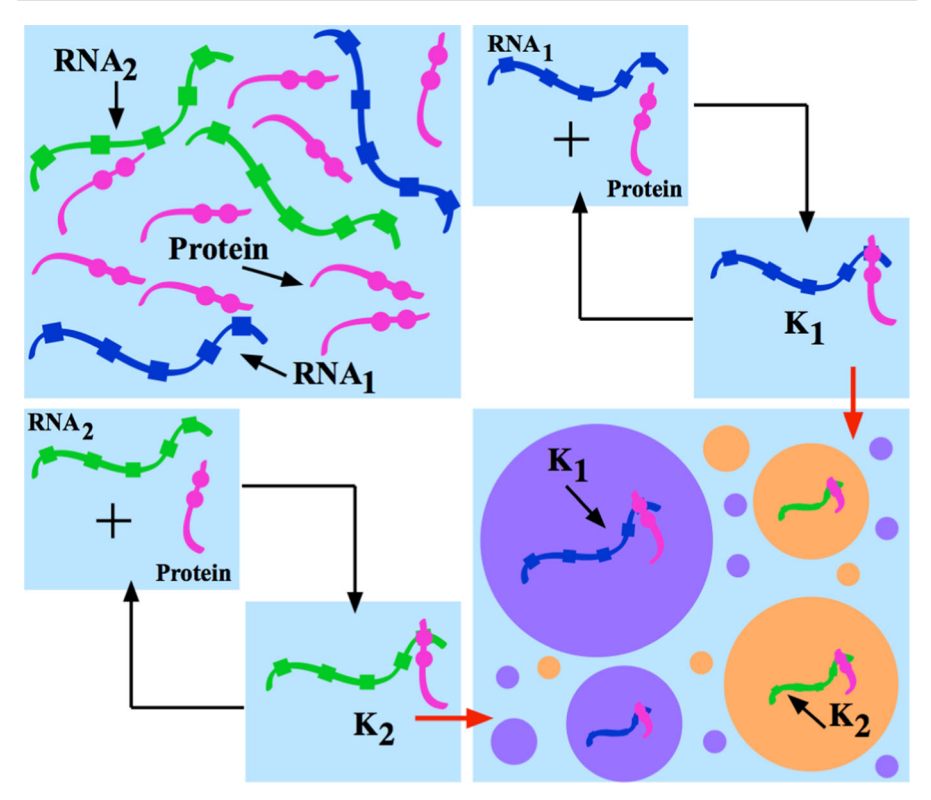


Fig. 1 (Color figure online) Diagram describing a biological system with two species of RNA competing for a pool of shared protein. The K_1 complex is formed when the first RNA (R_1) interacts with a free protein. Similarly, the K_2 complex is formed when the second RNA species (R_2) interacts with a free protein. Both protein–RNA complexes are capable of driving phase separation and forming distinct droplets

2 Model

We present a model that examines the sharing of a common protein-binding partner by multiple RNA species. While proteins and RNAs are capable of multivalent interactions, we assume for simplicity in this model that a reversible monovalent interaction occurs between each RNA and the protein species it binds with. As illustrated in Fig. 1, a single protein is capable of binding to an RNA from species 1 or 2 to form the K_1 or K_2 complex, and the complexes unbind at some rate. Each complex is capable of driving phase separation to form droplets.

As shown in Eqs. (1)–(8), this model couples the Cahn–Hilliard diffuse interface phase field model, the Flory–Huggins free energy scheme, and reversible protein–RNA interactions (under detailed balance) to describe the binding and unbinding of protein and RNA to form complexes capable of phase separation. The system evolves within a 2D rectangular domain $[0 L_x] \times [0 L_y]$, where L_x and L_y are the length in the x and y directions. Initially, we assume that there are no preformed protein–RNA complexes $(K_1(x, y, 0) = K_2(x, y, 0) = 0)$. The initial distribution of protein was



Parameter	Definition	Value	Units
λ_P	Diffusion rate of free protein	37.5×10^{-1}	μ m ² /s
λ_{R_1}	Diffusion rate of free RNA1	5.8×10^{-1}	μ m ² /s
λ_{R_2}	Diffusion rate of free RNA2	1.45×10^{-1}	μ m ² /s
λ_{K_1}	Diffusion rate of the K_1 complex	5×10^{-1}	μ m ² /s
λ_{K_2}	Diffusion rate of the K_2 complex	1.39×10^{-1}	$\mu m^2/s$
c_1	Binding rate of protein and RNA1 to form K_1	1.0×10^{0}	1/s
c_2	Disassociation rate of K_1	1.0×10^{-2}	1/s
c_3	Binding rate of protein and RNA2 to form K_2	1.0×10^{0}	1/s
c_4	Disassociation rate of K_2	1.0×10^{-2}	1/s
B_1	Scaled mobility of the K_1 complex in a droplet	2.97×10^{-3}	_
B_2	Scaled mobility of the K_2 complex in a droplet	4.45×10^{-3}	_

Table 1 Model parameter definitions

taken to be random. After discretizing the domain, the amount of protein at each grid point was initialized to independent and identically distributed samples from a uniform distribution between zero and one. As the two RNA species must compete for a shared pool of free protein, the initial amount of each RNA species across the entire domain was calculated to be half the initial amount of protein $(R_1 = R_2 = \frac{(1-P)}{2})$. Further, it is assumed that the total amount of protein and RNA are conserved, resulting in a system wherein K_1 and K_2 formation is limited by the initial conditions, such as would exist in an in vitro experiment. The parameter definitions are given in Table 1. The diffusion coefficients for P, R_1 , R_2 , K_1 , and K_2 were weighted against each other using the molecular weights of ~ 1600 nucleotide RNA (R_1) and ~4800 nucleotide RNA (R_2) , as well as a 78 kDa protein. We denote the volume fractions for the two protein–RNA complexes and the solvent as K_1 , K_2 , S, and we denote the non-dimensional concentrations of free protein and free RNAs as P, R_1 , and R_2 .

$$\frac{\partial K_1}{\partial t} = \nabla \cdot \left[\lambda_{N_1} M(K_1, K_2) \nabla \left(\frac{\delta F}{\delta K_1} \right) \right] + c_1 P R_1 - c_2 K_1 \tag{1}$$

$$\frac{\partial K_2}{\partial t} = \nabla \cdot \left[\lambda_{N_2} M(K_1, K_2) \nabla \left(\frac{\delta F}{\delta K_2} \right) \right] + c_3 P R_2 - c_4 K_2 \tag{2}$$

$$\frac{\partial P}{\partial t} = \nabla \cdot [\lambda_P M(K_1, K_2) \nabla P] - c_1 P R_1 + c_2 K_1 - c_3 P R_2 + c_4 K_2 \tag{3}$$

$$\frac{\partial R_1}{\partial t} = \nabla \cdot \left[\lambda_{R_1} M(K_1, K_2) \nabla R_1 \right] - c_1 P R_1 + c_2 K_1 \tag{4}$$

$$\frac{\partial R_2}{\partial t} = \nabla \cdot \left[\lambda_{R_2} M(K_1, K_2) \nabla R_2 \right] - c_3 P R_2 + c_4 K_2 \tag{5}$$



153 Page 6 of 16 K. Gasior et al.

$$F = \int_{\Omega} \left(\frac{\varepsilon^2}{2} \Big[|\nabla K_1|^2 + |\nabla K_2|^2 \Big] + A \cdot (K_1 \ln K_1 + K_2 \ln K_2 + S \ln S + \chi_{K_1 K_2} K_1 K_2 + \chi_{K_1 S} K_1 S + \chi_{K_2 S} K_2 S) \right) dx$$
(6)

$$K_1 + K_2 + S = 1 (7)$$

We impose reflecting boundary conditions on the boundary of the rectangular domain with

$$\nabla \frac{\delta F}{\delta K_1} \cdot \mathbf{n} = 0, \quad \nabla \frac{\delta F}{\delta K_2} \cdot \mathbf{n} = 0, \quad \nabla K_1 \cdot \mathbf{n} = 0, \quad \nabla K_2 \cdot \mathbf{n} = 0,$$

$$\nabla P \cdot \mathbf{n} = 0, \quad \nabla R_1 \cdot \mathbf{n} = 0, \quad \nabla R_2 \cdot \mathbf{n} = 0$$
(8)

This model also assumes that the binding of protein to RNA does not result in major structural changes that would impact the hydrodynamic radius and affect kinetic rates or diffusivities. However, $0 < M(K_1, K_2) \le 1$ is a mobility function that scales linearly with the volume fraction of each complex in a phase-dependent and complex-dependent manner, as shown in Eq. 9. With this mobility function, diffusion within the droplet is reduced by a factor of 10^3 compared to the surrounding matrix. Further, using the viscosities of two RNA complexes that share the same protein-binding partner (Zhang et al. 2015), the ratio of B_1 to B_2 is equal to $\left(\frac{K_2 \text{ Viscosity}}{K_1 \text{ Viscosity}}\right)$.

$$M(K_1, K_2) = (1 - (K_1 + K_2)) + B_1 K_1 + B_2 K_2.$$
(9)

In Eq. (6), F is the Flory–Huggins free energy, where A = 0.2 is a scaling factor and each χ is an interaction parameter (Weber et al. 2019). In particular, the parameters χ_{K_1S} , χ_{K_2S} , and $\chi_{K_1K_2}$ describe the mixing/de-mixing interactions between solute—solvent and solute—solute components. In Gasior et al. for simplicity, the solvent was not explicitly tracked, only mono- and bivalent protein–RNA complexes and their mixing energies. In the present model, the parameters χ_{K_1S} , χ_{K_2S} , and $\chi_{K_1K_2}$ control mixing kinetics between each complex and the solvent and between complexes. The logarithmic bulk potential in the Flory–Huggins free energy was regularized using the techniques developed in (Yang et al. 2018). We used a second-order finite-difference scheme for spatial discretization and second-order semi-implicit backward difference formula, as well as the stabilizing technique in (Shen and Yang 2010), for time discretization. Numerical schemes used are further outlined in Appendix A of (Gasior et al. 2019).

3 Results

We now explore the involvement of two classes of molecular interactions in the establishment and maintenance of a heterogeneous droplet field: the pairwise de-mixing energies (χ_{K_1S} , χ_{K_2S} , $\chi_{K_1K_2}$) and the association and dissociation rates of the two



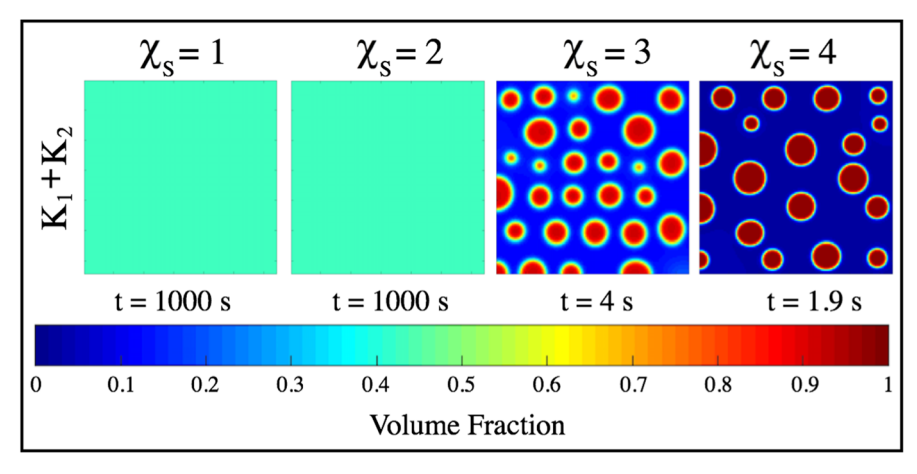


Fig. 2 (Colour figure online) Influence of the complex–solvent de-mixing energy on the behavior of the system. We assume: weak de-mixing of K_1 and K_2 , imposed by $\chi_{K_1K_2}=1$; the reversible molecular interaction rates are identical $(c_1=c_3,c_2=c_4)$; and, K_1 -solvent and K_2 -solvent de-mixing are equal, i.e., $\chi_{K_1S}=\chi_{K_2S}=\chi_S$. Once χ_S crosses the threshold value of $\chi_S=2.3$ the system can phase separate. Increases in χ_S shorten the time for phase separation and sharpen the interface between droplets and the surrounding matrix

RNA–protein complexes (c_i , i=1..4). We illustrate, by selected sampling of this 7-parameter space, how the development of a heterogeneous droplet field can arise consisting of both K_1 and K_2 droplets, two species of droplets that can coexist without allowing their components to co-localize within the same droplet space. We assume the complex–solvent de-mixing energies are equal ($\chi_{K_1S} = \chi_{K_2S} = \chi_S$). Recall that, in general, $\chi > 0$ indicates that the matrix acts as a poor solvent (Brangwynne et al. 2015; Berry et al. 2018), so that K_1 and K_2 favor de-mixing with solvent.

3.1 The Strength of Complex–Solvent De-Mixing Energy Allows for Phase Separation of Droplets

Figure 2 shows the influence of the complex–solvent de-mixing energy, χ_S . In this initial system, using the parameter values from Table 1, we assume a weak de-mixing energy between the K_1 and K_2 complexes ($\chi_{K_1K_2}=1$) and then examine the K_1+K_2 volume fraction. The reversible molecular interactions for K_1 and K_2 are identical ($c_1=c_3, c_2=c_4$), thus allowing both complexes to form and accumulate through time. For $0<\chi_S<2.3$, the de-mixing energy is insufficient for the complexes to phase separate from the solvent. Instead, as shown in Panels 1 and 2 of Fig. 2, we observe a well-mixed system. However, for $\chi_S\geq 2.3$, the de-mixing energy is sufficient for the system to phase separate, as shown in Fig. 2 Panel 3 with $\chi_S=3$. When increased further to $\chi_S=4$ (as in Fig. 2 Panel 4) the complexes separate faster, more completely from the solvent, with a sharper interface between the complex-rich droplets and the solvent.



153 Page 8 of 16 K. Gasior et al.

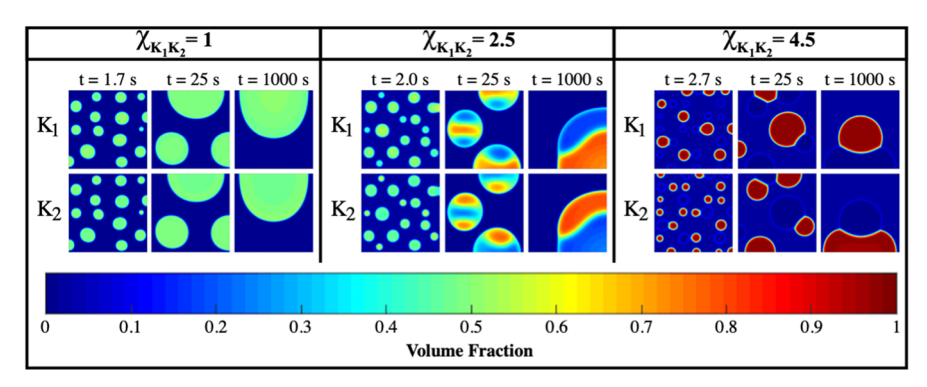


Fig. 3 (Color figure online) Using the binding dynamics from Table 1 and $\chi_S = 4.25$, we examine the effect of the K_1 – K_2 de-mixing energy ($\chi_{K_1K_2}$) on droplet composition. For $\chi_{K_1K_2} = 1$, the system has well-mixed droplets with equal amounts of K_1 and K_2 occupying the same droplets at the time of phase separation. With $\chi_{K_1K_2} = 2.5$, K_1 and K_2 are well mixed within the same droplets at the time of phase separation but undergo asymmetric organizational changes as time increases. This asymmetric organization is then maintained long term (up to t = 1000 s). Finally, for $\chi_{K_1K_2} = 4.5$, there are distinct K_1 and K_2 droplets at the onset of phase separation. As the system evolves, it maintains a heterogeneous droplet field at t = 1000 s and does not ripen into a single droplet state

3.2 The Strength of the K_1 – K_2 De-Mixing Energy Establishes Distinct Droplets Unique to the RNA Species Involved in RNA–Protein Complex Formation

To achieve a system wherein the K_1 and K_2 complexes form and maintain their own individual droplets, $\chi_{K_1K_2}$ must be sufficiently large so as to exclude the competing protein–RNA complex species. Using the results from Fig. 2, we assume a strong demixing energy between a complex and the solvent ($\chi_S = 4.25$), and we use identical reversible molecular interactions for K_1 and K_2 formation, as defined in Table 1. For a low value of $\chi_{K_1K_2}$ ($\chi_{K_1K_2} = 1$), there is a weak de-mixing energy between the K_1 and K_2 complexes. With this inter-complex de-mixing energy, both complexes share the same droplets, as shown in Fig. 3, Panel 1. At an intermediate value of $\chi_{K_1K_2}$ ($\chi_{K_1K_2} = 2.5$), K_1 and K_2 initially occupy the same droplet but exhibit asymmetric protein–RNA complex organization as the protein–RNA complexes accumulate and fail to fully separate themselves (Fig. 3, Panel 2). Finally, high values of $\chi_{K_1K_2}$ ($\chi_{K_1K_2} = 4.5$) the two complexes form separate droplets (Fig. 3, Panel 3).

Figure 4 further highlights how the K_1 – K_2 de-mixing energy affects the distribution of the two complexes within the same droplet. Using the droplet systems from Fig. 3 at t=1000 s, Fig. 4 examines a cross section of the K_1+K_2 volume fraction. As $\chi_{K_1K_2}$ increases, the overlap of the K_1 and the K_2 volume fractions decreases until, at $\chi_{K_1K_2}=4.5$, the system achieves a complete exclusion and separation of K_1 and K_2 into distinct droplets.



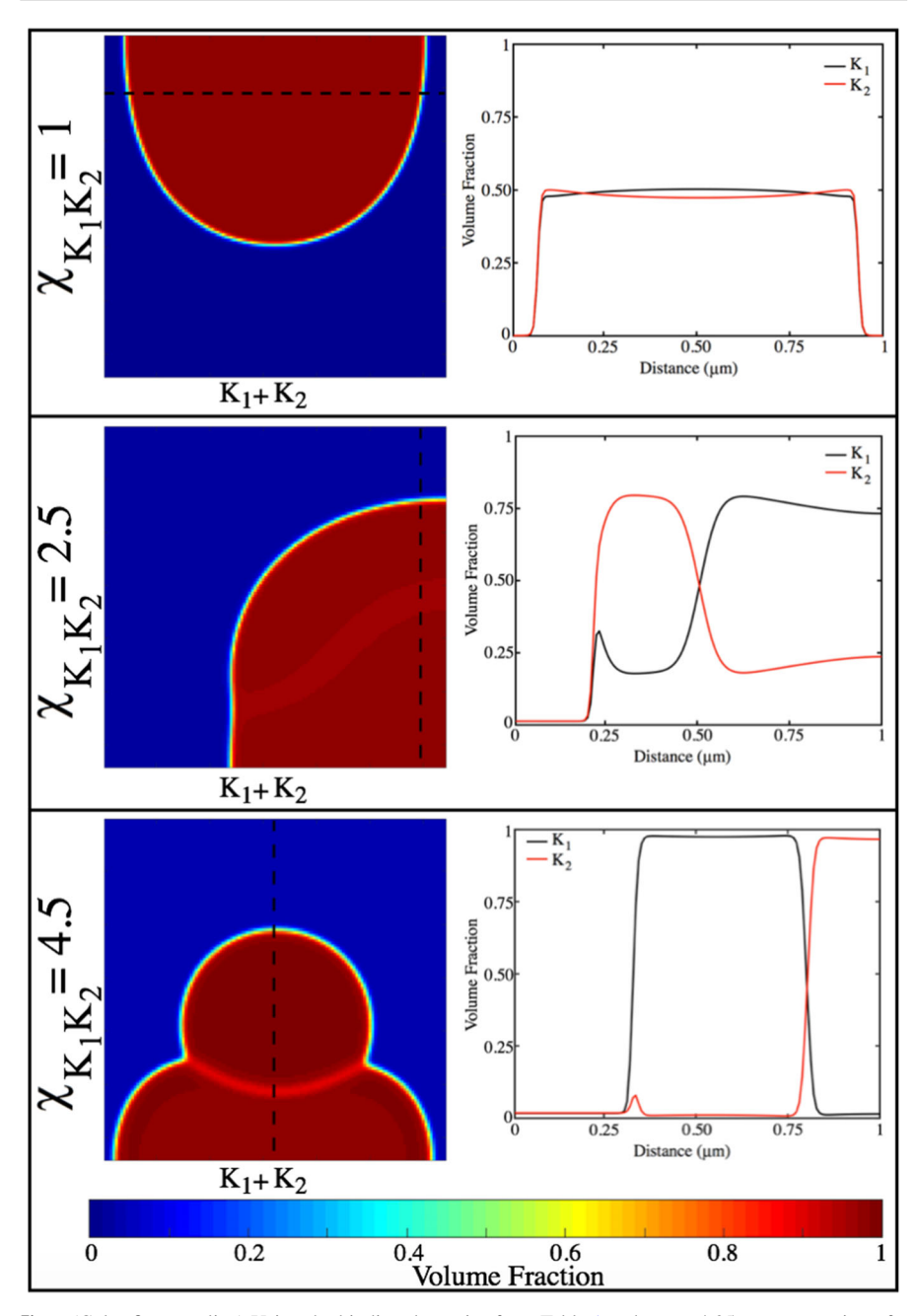


Fig. 4 (Color figure online) Using the binding dynamics from Table 1 and $\chi_S = 4.25$, a cross section of a droplet at t = 1000 s is shown. For $\chi_{K_1K_2} = 1$, K_1 and K_2 mix within a single droplet. For $\chi_{K_1K_2} = 2.5$, the two complexes begin to separate from each other but cannot form two separate droplets. For $\chi_{K_1K_2} = 4.5$, K_1-K_2 interactions are sufficiently unfavorable that they form distinct droplets with a shared interface



153 Page 10 of 16 K. Gasior et al.

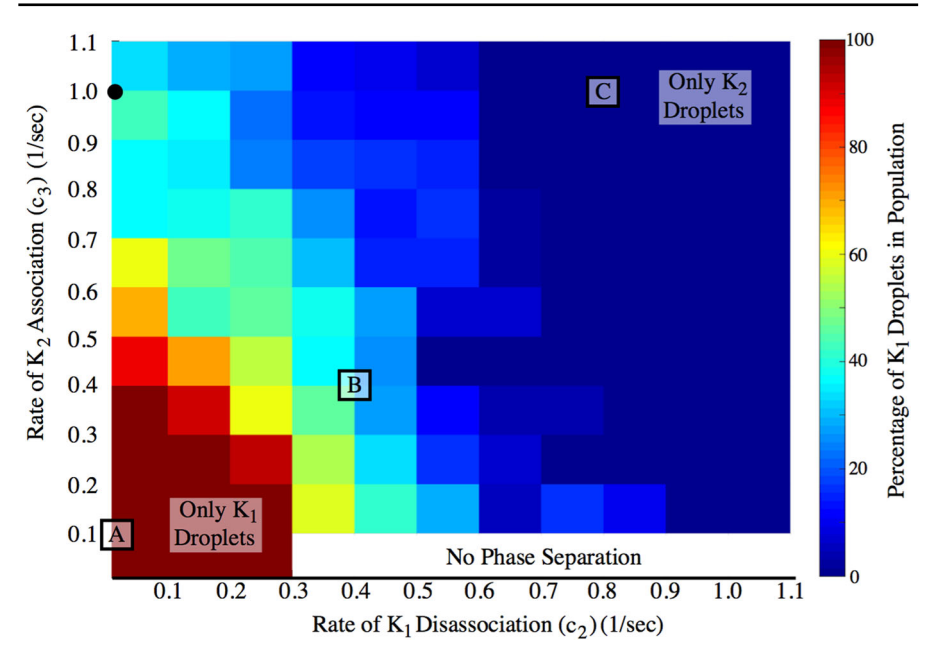


Fig. 5 (Color figure online) The total population of droplets is comprised of K_1 and K_2 droplets. This state diagram examines the influence of reversible molecular interactions on the percentage of K_1 droplets at the time of phase separation (with $\chi_S = 4.25$ and $\chi_{K_1K_2} = 4.5$). This state diagram contains four sections of behavior. For high values of c_2 and low values of c_3 , the system is unable to phase separate. For low values of c_2 and c_3 , there is a homogeneous droplet field of only K_1 droplets at the time of phase separation. Conversely, high values of both c_2 and c_3 produce a homogeneous droplet field of only K_2 droplets. But, for intermediate values of c_2 and c_3 , we observe a transitional area wherein the percentage of K_1 droplets present in the droplet field is between 0 and 100%. For reference, the droplet field explored in Figs. 3 and 4 is marked with a black dot. Representative examples marked with A, B, and C are shown in Fig. 6

3.3 Reversible Molecular Interactions Control Time Scale and Emergence of Droplet Field Heterogeneity

While the K_1 – K_2 de-mixing energy ($\chi_{K_1K_2}$) plays a crucial role in separating the two protein–RNA complexes into distinct droplets, the reversible molecular interactions between the protein and the RNA are equally important in establishing a heterogeneous droplet field. Using sufficiently high complex–solvent and K_1 – K_2 de-mixing energies ($\chi_S = 4.25$, $\chi_{K_1K_2} = 4.5$), Figs. 5 and 6 explore how different RNAs are able to establish a heterogeneous droplet field despite the fact that they share the same binding partner: free protein (P). Due to the monovalent nature of the protein and RNA interactions in this model, it is sufficient to examine two of the four reversible molecular interaction rates: we have chosen c_2 and c_3 . Values for c_1 and c_4 from Table 1 indicate that K_1 is a quick-to-form complex while K_2 is slow to dissociate. Varying c_2 and c_3 allows us to understand how sharing of the free protein between the two complexes can tune the dynamics of phase separation and the emergence of distinct droplet species.



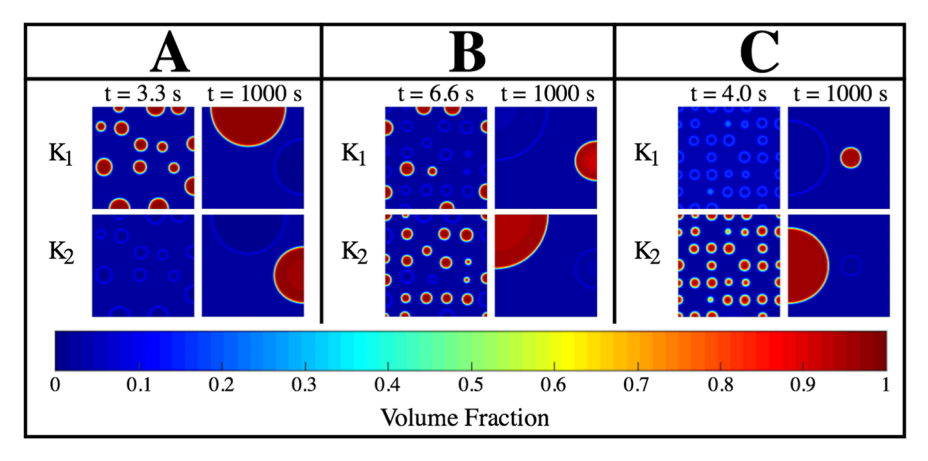


Fig. 6 (Color figure online) Three representative examples are shown (marked as a, b, and c in Fig. 5). For binding dynamics that favor the formation of one complex over the other, such as K_1 in system **a** and K_2 in system c, we see only one type of protein–RNA complex in the droplet field at the onset of phase separation. Systems that exist in the intermediate region of Fig. 5, such as \mathbf{b} , have both K_1 and K_2 droplets at the onset of phase separation. Note that, even if a system only has one type of droplet at the onset of phase separation, latent droplets of the other species can form, creating a long term heterogeneous droplet field, as in systems a and c

Figure 5 presents a state diagram of the percentage of K_1 droplets in the droplet field at the time of phase separation. Three regimes are indicated (A, B, and C) in Fig. 5, each of which is illustrated in Fig. 6. For different values of c_2 and c_3 , there are four general behaviors that this system can adopt. If the rate of dissociation for K_1 (c_2) is too high while, simultaneously, the rate of association for K_2 (c_3) is too low, a sufficient level of complex is never reached, and the system will not phase separate. For low values of c_2 and c_3 — where the K_1 complex breaks apart slowly, and the K_2 complex forms slowly— there is a homogeneous droplet field of only K_1 droplets at the time of phase separation (an example of this is shown in Fig. 6a). Conversely, for high values of both c_2 and c_3 — when the both complexes are quick to form, the K_1 complex is unstable, and the K_2 complex is stable—there is a homogeneous droplet field of only K_2 droplets at the time of phase separation (an example of this is shown in Fig. 6c). But, for intermediate values of c_2 and c_3 (like the system presented in Fig. 6b), the percentage of K_1 droplets present in the droplet field at the time of phase separation varies between 0 and 100%. In this intermediate regime, the exchange of free protein creates a heterogeneous droplet field at the time of phase separation.

3.4 Phase Separation Can Occur on Multiple Time Scales

Even if a system does not start out as a heterogeneous mixture of K_1 and K_2 droplets at the time of phase separation, it is possible for the system to become one in the long term. One example of this is shown in Fig. 6a, where the K_1 complex is quickto-form and stable while the K_2 complex is slow-to-form and stable. At the time of phase separation, there are only K_1 droplets in the system. But, as time evolves, the



 K_2 complex accumulates and, eventually, a K_2 droplet forms. Further, the formation of this new K_2 droplet establishes a heterogeneous droplet field with 1 droplet of each protein–RNA complex species in the long term ($t=1000 \, \mathrm{s}$). Similar behavior is observed in Fig. 6c but, in this case, it is the K_2 complex that drives phase separation and the K_1 complex droplets slowly emerge over time. Therefore, it is the binding dynamics for the formation of K_1 and K_2 that determine the latent appearance and overall time scale for the formation of distinct and coexisting K_1 and K_2 droplets when the K_1 – K_2 de-mixing energy is sufficiently high.

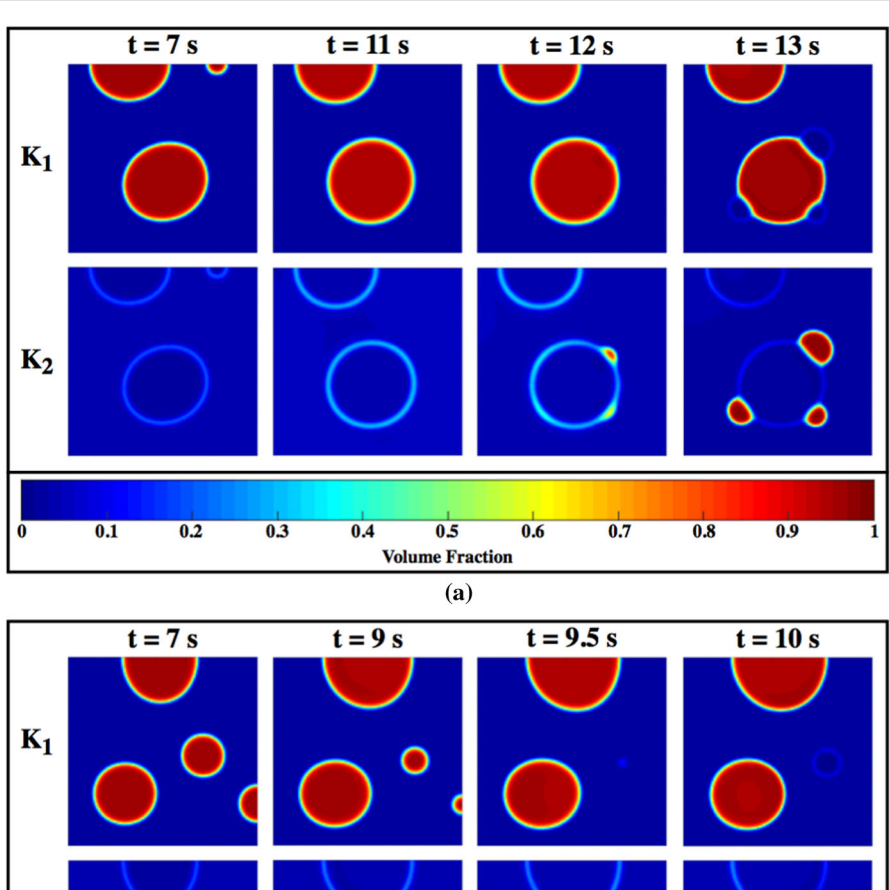
The latent appearance of a second droplet species can occur through one of two methods in the system. Using the binding dynamics featured in Fig. 6a, Fig. 7 outlines these two potential methods: budding and Ostwald ripening. In Fig. 7a, the K_1 droplets sequester much of the protein during the initial phase separation and droplet formation. As time progresses, R_2 binds with the free protein as it escapes the K_1 droplets, allowing the accumulation of K_2 at the surface of the K_1 droplets. Over time, K_2 continues to build up but cannot mix into the K_1 droplet due to the high $\chi_{K_1K_2}$ value. Instead, the accumulated K_2 ultimately buds off the K_1 droplet to form a separate K_2 droplet that still shares an interface with the initial K_1 droplet. Figure 7b highlights the second method of latent droplet formation. As the system matures, K_2 continues to build up at the interface between the K_1 droplets and the surrounding cytosol. With Ostwald ripening of K_1 droplets, the smaller K_1 droplets dissipate and the K_2 on the surface becomes highly concentrated, allowing it to form a standalone droplet in the space previously occupied by the shrinking K_1 droplet. Hence, K_1 droplets effectively nucleate the formation of K_2 droplets without initially sharing a boundary.

4 Discussion

In this work, we have shown how different parameters can be tuned to create and maintain a stable, heterogeneous droplet field wherein two droplets with distinct molecular complexes can co-exist. Alternatively, the distinct molecular complexes can co-exist within the same droplet, or the complexes can be sequestered in separate droplets that are attached via a shared interface. While strong interaction energies cause the distinct protein–RNA complexes to de-mix from both the surrounding matrix and from each other, it is the relative timescales of the reversible molecular binding rates that dictate the dominance of specific complexes and whether their distinct droplets coexist to create a heterogeneous droplet field. These parameters have physiological relevance in cells through variable binding affinities of proteins for different RNAs, depending on the valency and structure of RNAs.

In a de-mixed system, there are two general sets of reversible molecular interactions that can result in a droplet field occupied by two species of protein–RNA droplets. Either of these interaction rates indicate a system where there is true competition for the free protein so both complexes can accumulate and drive phase separation, or, a single protein–RNA species dominates at the time of phase separation, followed by the later appearance of a second droplet species due to the slow accumulation of the second RNA–protein complex. This latent droplet formation can occur at the interface of a droplet from the competing RNA–protein complex species via budding or at the





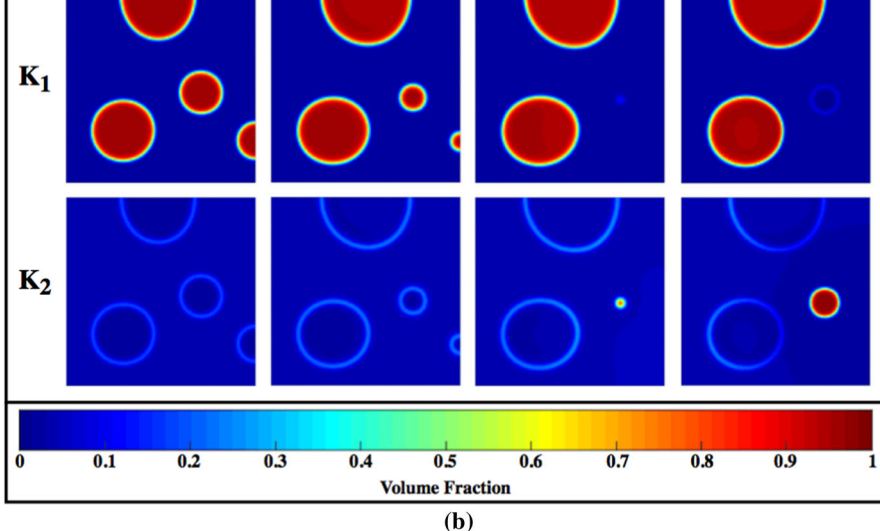


Fig. 7 (Color figure online) Using the binding dynamics from system $\bf a$ in Figs. 5 and 6, we show two different ways a homogeneous droplet field can develop into a heterogeneous droplet field. In both ($\bf a$) and ($\bf b$), only K_1 droplets are formed at the time of phase separation. $\bf a$ As the K_2 complex continues to accumulate, it builds up at the interface between the K_1 droplets and the matrix. Due to the high $\chi_{K_1K_2}$ value, the K_2 complex cannot mix into the K_1 droplets. Therefore, after enough K_2 has accumulated, separate K_2 droplets bud off the interface of the K_1 droplets. $\bf b$ As smaller K_1 droplets undergo Ostwald ripening, they bring the K_2 at the interface into close proximity. The K_2 can then concentrate itself and form a droplet where the smaller K_1 droplet once was. As time progresses and the K_1 droplets continue to undergo Ostwald ripening, the single K_2 droplet continues to grow



153 Page 14 of 16 K. Gasior et al.

site of a dissipating smaller droplet from the competing species as Ostwald ripening occurs. In both cases, the interface of the protein–RNA droplet becomes important for the accumulation of its competitor: this interface is where the competing protein–RNA complex can accumulate until it is capable of forming its own droplet. Further, although the dissipation of a droplet from one species can give rise to a stand-alone droplet of the competing species, if two droplets of competing protein–RNA species eventually come in contact with each other, they will continue to share that interface rather than breaking apart.

Droplet species that share a portion of their interface could be a mechanism to prolong the stability of smaller droplets. Without an energy input or an emulsifier, the system will eventually reach a state with a single droplet for each species. There are two main factors that lead to a decrease in droplet number: droplet merging and Ostwald ripening. An active area of investigation for how droplets might be stabilized is through arrest of Ostwald ripening by way of non-equilibrium chemical reactions or gelation. While interface sharing is not sufficient to stabilize droplet size and number, our results show it is an alternative mechanism to transiently stabilize a droplet field.

When two RNA species compete for a shared pool of free protein as their common binding partner, the establishment of a shared interface between distinct and different droplets could potentially enhance or inhibit resource access for each protein–RNA complex species. Within the model, diffusion of components in the surrounding matrix is on the order of 10³ times higher than it is within the droplet environment. Two droplets sharing an interface and limiting the contact each has with the surrounding matrix could ultimately limit the availability of resources and subsequently limit the formation of additional complexes. Or, conversely, this bumper-to-bumper behavior of the droplets could nucleate the formation of additional complexes by locally concentrating free protein. Determining the effect of boundary sharing behavior on a system with competing protein–RNA species will be crucial: the localization and segregation of free protein that is needed by both complexes could ultimately promote or inhibit necessary intra-droplet biochemical interactions that lead to larger macroscopic changes.

Acknowledgements Kelsey Gasior was supported in part by NSF DMS-1816630. M. Gregory Forest was supported in part by NSF DMS-1816630, DMS-1517274, and DMS-1664645. Amy Gladfelter was supported in part by NIH GM R01-GM081506. Jay M. Newby was supported by the Natural Sciences and Engineering Research Council of Canada (RGPIN-2019-06435, RGPAS-2019-00014, DGECR-2019-00321) and the NSF (DMS-171474, DMS-1816630).

Funding Kelsey Gasior was supported in part by NSF DMS-1816630. M. Gregory Forest was supported in part by NSF DMS-1816630, DMS-1517274, and DMS-1664645. Amy Gladfelter was supported in part by NIH GM R01-GM081506. Jay M. Newby was supported by the Natural Sciences and Engineering Research Council of Canada (RGPIN-2019-06435, RGPAS-2019-00014, DGECR-2019-00321) and the NSF (DMS-171474, DMS-1816630).

Data Availability All simulation data available on request.



Compliance with Ethical Standards

Conflict of interest The authors declare that they have no competing interests.

Code Availability Code was created using Matlab.

References

- Banani SF, Lee HO, Hyman AA, Rosen MK (2017) Biomolecular condensates: organizers of cellular biochemistry. Nat Rev Mol Cell Biol 18(5):285-298
- Berry J, Brangwynne CP, Haataja M (2018) Physical principles of intracellular organization via active and passive phase transitions. Rep Prog Phys 81(4):046601
- Brangwynne CP, Tompa P, Pappu RV (2015) Polymer physics of intracellular phase transitions. Nat Phys 11(11):899-904
- Cahn JW, Hilliard JE (1958) Free energy of a nonuniform system. I. Interfacial free energy. J Chem Phys 28(2):258-267
- Chong PA, Vernon RM, Forman-Kay JD (2018) RGG/RG motif regions in RNA binding and phase separation. J Mol Biol 430(23):4650-4665
- Dudowicz J, Freed KF, Douglas JF (2004) Flory-Huggins model of equilibrium polymerization and phase separation in the Stockmayer fluid. Phys Rev Lett 92(4):045502
- Elbaum-Garfinkle S, Kim Y, Szczepaniak K, Chen CC-H, Eckmann CR, Myong S, Brangwynne CP (2015) The disordered P granule protein LAF-1 drives phase separation into droplets with tunable viscosity and dynamics. Proc Natl Acad Sci 112(23):7189-7194
- Feric M, Vaidya N, Harmon TS, Mitrea DM, Zhu L, Richardson TM, Kriwacki RW, Pappu RV, Brangwynne CP (2016) Coexisting liquid phases underlie nucleolar subcompartments. Cell 165(7):1686–1697
- Gasior K, Zhao J, McLaughlin G, Forest MG, Gladfelter AS, Newby J (2019) Partial demixing of RNAprotein complexes leads to intradroplet patterning in phase-separated biological condensates. Phys Rev E 99(1):012411
- Gladfelter AS (2006) Nuclear anarchy: asynchronous mitosis in multinucleated fungal hyphae. Curr Opin Microbiol 9(6):547-552
- Glotzer SC, Di Marzio EA, Muthukumar M (1995) Reaction-controlled morphology of phase-separating mixtures. Phys Rev Lett 74(11):2034
- Hult C, Adalsteinsson D, Vasquez PA, Lawrimore J, Bennett M, York A, Cook D, Yeh E, Forest MG, Bloom K (2017) Enrichment of dynamic chromosomal crosslinks drive phase separation of the nucleolus. Nucleic Acids Res 45(19):11159-11173
- Hyman AA, Weber CA, Jülicher F (2014) Liquid-liquid phase separation in biology. Annu Rev Cell Dev Biol 30:39-58
- Langdon EM, Gladfelter AS (2018) A new lens for RNA localization: liquid-liquid phase separation. Annu Rev Microbiol 72:255-271
- Langdon EM, Qiu Y, Niaki AG, McLaughlin GA, Weidmann C, Gerbich TM, Smith JA, Crutchley JM, Termini CM, Weeks KM (2018) mRNA structure determines specificity of a polyQ-driven phase separation. Science 360:922-927
- Lee C, Zhang H, Baker AE, Occhipinti P, Borsuk ME, Gladfelter AS (2013a) Protein aggregation behavior regulates cyclin transcript localization and cell-cycle control. Dev Cell 25(6):572-584
- Lee CF, Brangwynne CP, Gharakhani J, Hyman AA, Jülicher F (2013b) Spatial organization of the cell cytoplasm by position-dependent phase separation. Phys Rev Lett 111(8):088101
- Lee C, Occhipinti P, Gladfelter AS (2015) PolyQ-dependent RNA-protein assemblies control symmetry breaking. J Cell Biol 208:533-544
- Lin Y, Protter DS, Rosen MK, Parker R (2015) Formation and maturation of phase-separated liquid droplets by RNA-binding proteins. Mol Cell 60(2):208-219
- Molliex A, Temirov J, Lee J, Coughlin M, Kanagaraj AP, Kim HJ, Mittag T, Taylor JP (2015) Phase separation by low complexity domains promotes stress granule assembly and drives pathological fibrillization. Cell 163(1):123-133



153 Page 16 of 16 K. Gasior et al.

Pak CW, Kosno M, Holehouse AS, Padrick SB, Mittal A, Ali R, Yunus AA, Liu DR, Pappu RV, Rosen MK (2016) Sequence determinants of intracellular phase separation by complex coacervation of a disordered protein. Mol Cell 63(1):72–85

Qin R, Bhadeshia H (2010) Phase field method. Mater Sci Technol 26(7):803-811

Schaefer MH, Wanker EE, Andrade-Navarro MA (2012) Evolution and function of CAG/polyglutamine repeats in protein–protein interaction networks. Nucleic Acids Res 40(10):4273–4287

Shen J, Yang X (2010) Numerical approximations of allen-cahn and cahn-hilliard equations. Discrete Contin Dyn Syst 28(4):1669-1691

Tetz G, Tetz V (2017) Prion-like domains in phagobiota. Front Microbiol 8:2239

Walker B, Taylor D, Lawrimore J, Hult C, Adalsteinsson D, Bloom K, Forest MG (2019) Transient crosslinking kinetics optimize gene cluster interactions. PLoS Comput Biol 15(8):e1007124

Weber CA, Zwicker D, Jülicher F, Lee CF (2019) Physics of active emulsions. Rep Prog Phys 82(6):064601
Yang X, Zhao J, He X (2018) Linear, second order and unconditionally energy stable schemes for the viscous Cahn–Hilliard equation with hyperbolic relaxation using the invariant energy quadratization method. J Comput Appl Math 343:80–97

Zhang H, Elbaum-Garfinkle S, Langdon EM, Taylor N, Occhipinti P, Bridges AA, Brangwynne CP, Gladfelter AS (2015) RNA controls PolyQ protein phase transitions. Mol Cell 60(2):220–230

Zwicker D, Seyboldt R, Weber CA, Hyman AA, Jülicher F (2017) Growth and division of active droplets provides a model for protocells. Nat Phys 13(4):408

Publisher's Note Springer Nature remains neutral with regard to jurisdictional claims in published maps and institutional affiliations.

Affiliations

K. Gasior^{1,2} · M. G. Forest^{2,3,4} · A. S. Gladfelter⁵ · J. M. Newby⁶

K. Gasior kgasior@fsu.edu

M. G. Forest forest@unc.edu

- Department of Mathematics, Florida State University, 1017 Academic Way, Tallahassee, FL 32304, USA
- Department of Mathematics, University of North Carolina at Chapel Hill, 329 Phillips Hall CB #3250, Chapel Hill, NC 27514, USA
- Joint Department of Biomedical Engineering, University of North Carolina at Chapel Hill and North Carolina State University, 333 S Columbia Street, Chapel Hill, NC 27514, USA
- Department of Applied Physical Sciences, University of North Carolina at Chapel Hill, 1112 Murray Hall, CB #3050, Chapel Hill, NC 27514, USA
- Department of Biology, University of North Carolina at Chapel Hill, Coker Hall CB #3280, 120 South Road, Chapel Hill, NC 27514, USA
- Department of Mathematical and Statistical Sciences, CAB 632, University of Alberta, Edmonton, AB T6G 2G1, Canada

